APL Photonics

Effective-medium-clad Bragg grating filters

Cite as: APL Photonics **6**, 076105 (2021); https://doi.org/10.1063/5.0051310
Submitted: 24 March 2021 . Accepted: 07 July 2021 . Published Online: 20 July 2021

Weijie Gao, Wendy S. L. Lee, Christophe Fumeaux, et al.

Effective-medium-clad Bragg grating filters

Cite as: APL Photon. 6, 076105 (2021); doi: 10.1063/5.0051310
Submitted: 24 March 2021 • Accepted: 7 July 2021 •
Published Online: 20 July 2021

Weijie Gao,[a] Wendy S. L. Lee,[b] Christophe Fumeaux, and Withawat Withayachumnankul[c]

AFFILIATIONS

Terahertz Engineering Laboratory, School of Electrical and Electronic Engineering, The University of Adelaide, Adelaide, SA 5005, Australia

[a]**Electronic mail:** weijie.gao@adelaide.edu.au
[b]**Current address:** Department of Electrical and Electronic Engineering, The University of Melbourne, Parkville, Victoria 3010, Australia.
[c]**Author to whom correspondence should be addressed:** withawat@adelaide.edu.au

ABSTRACT

We propose a series of integrated Bragg grating filters with performance enhancement via the concept of effective medium. The bandstop filters are built in a high-resistivity silicon wafer and operated over the WR-3.4 band (220–330 GHz) with in-plane polarization. The proposed designs use an additional degree of freedom in controlling the effective refractive index so as to fully use the potential of the Bragg grating structures. As a result, the high insertion loss typically observed at the low-frequency bound of the filters due to weak wave confinement can be reduced, while radiation caused by the leaky-wave effect at the high-frequency bound is minimized, allowing for a 40% operation fractional bandwidth. These features are not achievable with conventional waveguide Bragg grating filters. All-silicon prototypes of filter samples are experimentally validated, demonstrating promising performance for a wide range of terahertz applications. The techniques to improve the filter characteristics by controlling the effective medium can be adopted in both microwave and optics domains.

I. INTRODUCTION

Terahertz integrated systems have attracted great attention for their compactness, portability, and low cost compared to conventional quasi-optical systems while promising a wide range of applications from imaging to communications.[1,2] In particular, technologies from both electronics and photonics have accelerated the progress in forming terahertz integrated circuits, enabling comprehensive functionalities from signal generation, transmission, and processing to detection with moderately high efficiency.[1] To this end, terahertz integrated waveguides with high efficiency, low dispersion, and broad bandwidth are indispensable. Recently, we have proposed a class of substrate-free all-silicon effective-medium-clad dielectric waveguides with a measured average loss of 0.075 dB/cm, a group velocity dispersion of around ± 10 ps/(THz mm), and a fractional bandwidth of 40% over 220–330 GHz while supporting two orthogonal fundamental modes.[3] High-speed terahertz communications with a real-time transmission data rate of up to 30 Gbit/s were demonstrated on a straight waveguide.[4] Meanwhile, a series of elementary components, including bendings, crossovers, and directional couplers, have been reported as building blocks for a terahertz integrated platform.[3] However, filters, as one of the most essential components for terahertz integrated circuits, are still not available on this platform. In line with the practical needs of wideband terahertz systems, we are motivated in this work to investigate filters based on the effective-medium-clad waveguide platform.[5]

To realize passive filters, one common approach is to periodically alternate high and low impedance segments or equivalently high and low modal indices along a guiding structure. This allows us to effectively control the interference in transmitted and reflected waves, thus generating the desired stopband or passband response over a particular frequency band.[6,7] Accordingly, a number of terahertz filters based on microwave[8–10] and optical[11–13] waveguiding structures have been proposed. However, microwave-technology-based filters suffer from high metallic loss at terahertz bands. An exception includes rectangular waveguide based filters[9] which achieve relatively low loss due to low current density on metal. Nevertheless, the manufacturing complexity of metallic waveguide filters increases significantly with frequency, while their bulky form factor is not compatible to integrated systems. From the optics side, thin-film filters consisting of multi-layer dielectrics[11] are also not

integratable despite their structural and design simplicity. Furthermore, although one dimensional photonic crystal cavities[13] have good integrability, the passband has significant fluctuations resulting from the strong refractive index contrast between air and silicon. In addition, the 3-dB bandwidth tends to be large due to the same reason, thus limiting designability. Recently, a Bragg grating filter based on a polymer rib waveguide was proposed.[12] This filter features structural simplicity; however, it lacks a supporting structure for integration. Similar to the concept of Bragg grating structure, an optical bandstop filter realized by varying the parasitic elements along a waveguide core was reported.[14] However, its rejection performance was modest, while the passband response exhibited significant ripples.

In essence, all open dielectric waveguide-based Bragg filters suffer from limits in broadband operation, much needed for terahertz applications. The insertion loss increases with increasing frequency because of radiation resulting from the grating period close to one guided wavelength.[15] Moreover, the transmission levels at lower frequencies tend to be reduced due to weak wave confinement of guided waves. These effects limit the filter operation bandwidth, which is generally not an issue for typical narrow-band operation at optical frequencies, e.g., with a relative bandwidth of around 2.3% at the C-band or 3.8% at the L-band. In contrast, these effects become an issue at a terahertz band, which occupies a much larger fractional bandwidth, e.g., 40% for the WR-3.4 band. Therefore, it is impractical to directly scale the existing optical waveguide Bragg grating filters down to the terahertz frequency band.

In this work, we present a class of terahertz Bragg grating filters based on our recently proposed effective-medium-clad waveguide.[3,4] This waveguide platform allows the modal index to be modified by varying the waveguide core dimensions and/or the cladding configuration. Compared to conventional filters with physical corrugation of the waveguide core,[16–18] this technique offers an additional level of flexibility to control the filter characteristics, e.g., reducing insertion loss and allowing for broadband operation with a compact footprint. These features are very desirable in terahertz applications that typically leverage a vast available bandwidth with limited source power. This work is organized as follows: the design principles and considerations to select filter dimensions are given in Sec. II, while the filter characteristics including transmission performance, bandwidth, central frequencies, and dispersion are presented in Sec. III followed by the conclusion in Sec. IV.

II. DESIGN PRINCIPLES

A. Overview

As shown in Fig. 1(a), the proposed Bragg grating filter is built in a substrateless effective-medium-clad dielectric waveguide, which consists of a silicon waveguide core and in-plane effective medium claddings with lower relative permittivity, allowing for waveguiding through total internal reflection. The claddings are realized by periodically perforating the silicon slab with subwavelength spacing. Consequently, based on the Maxwell–Garnett effective medium theory,[19] the effective relative permittivity tensor of the cladding material can be locally controlled by adjusting the lattice parameters, namely, the hole diameter d and lattice period a. The Bragg gratings are realized by corrugating the waveguide core laterally in a period of Λ, which is equal to half the Bragg wavelength, i.e.,

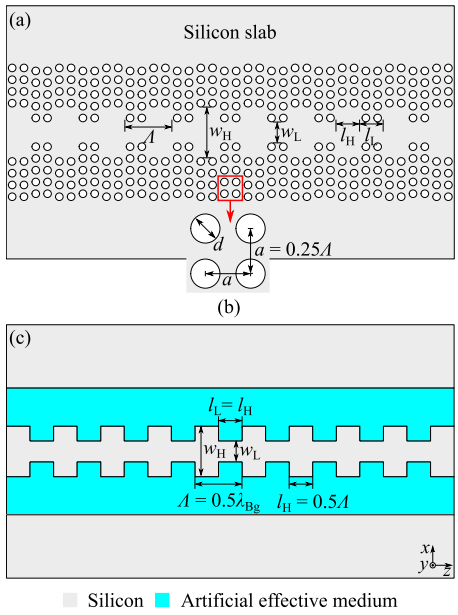

FIG. 1. Effective-medium-clad Bragg grating filter. (a) The filter cladded by an air–silicon effective medium realized by perforating the silicon slab. (b) A magnified view of effective medium cladding in a square lattice with a perforation period a and a hole diameter d. (c) The same filter with the cladding replaced by artificial anisotropic material. The artificial material is equivalent to the air–silicon effective medium with an effective relative permittivity tensor (ϵ_x, ϵ_y, ϵ_z) = (6.642, 8.193, 6.642). The realized filter is based on a 250 μm thick high-resistivity intrinsic float-zone silicon wafer with a relative permittivity ϵ_{Si} = 11.68. The unpatterned silicon slab is for handling purpose.

the central operation wavelength of the Bragg grating filter. Importantly, the proposed Bragg grating filter has access to an additional degree of freedom by varying the cladding to modify the modal indices of the gratings. We will show through various designs that this additional control of the effective-medium claddings can yield benefits in terms of passband transmission levels, stop-band bandwidth, and device footprint.

B. Design consideration

Initially, a simple uniform Bragg grating filter is implemented on the effective-medium-clad waveguide platform. In this work, we design the Bragg grating filter based on a single 250 μm thick high-resistivity silicon wafer with a relative permittivity ϵ_{Si} = 11.68 and resistivity of >10 kΩ cm. The filter is designed to operate in the E_{11}^x mode with in-plane polarization, which is compatible with most of the available terahertz devices. The full-wave simulations are performed with CST Microwave Studio 2019, where a realistic loss tangent of 3×10^{-5} is adopted for the silicon material. To save computational resources, as shown in Fig. 1(c), homogeneous cladding materials are adopted in simulations for initial investigations. It is noted that due to the approximations of the cladding relative permittivity used in the simulations, the calculated parameters (Λ, a, and d) need to be slightly optimized for the final design.

A critical step is to properly select the waveguide width for each section and to control the relative permittivity tensor (ϵ_x, ϵ_y, ϵ_z) of

the effective medium claddings. This tensor is determined by the perforation period a and hole diameter d and can be calculated based on the Maxwell–Garnett effective medium theory as[19]

$$\epsilon_x = \epsilon_{\mathrm{Si}} \frac{(\epsilon_{\mathrm{air}} + \epsilon_{\mathrm{Si}}) + (\epsilon_{\mathrm{air}} - \epsilon_{\mathrm{Si}})\zeta}{(\epsilon_{\mathrm{air}} + \epsilon_{\mathrm{Si}}) - (\epsilon_{\mathrm{air}} - \epsilon_{\mathrm{Si}})\zeta}, \tag{1}$$

$$\epsilon_y = \epsilon_{\mathrm{Si}} + (\epsilon_{\mathrm{air}} - \epsilon_{\mathrm{Si}})\zeta, \tag{2}$$

$$\epsilon_z = \epsilon_x, \tag{3}$$

where ζ represents the fill factor of the air volume in silicon. For a square lattice, the fill factor can be calculated from $(\pi d^2)/(4a^2)$. Since the filter operates in the E_{11}^x mode with in-plane polarization, only ϵ_{x} is considered for the cladding relative permittivity to calculate the waveguide modal index. The average modal index $n_{\mathrm{eff}} = (n_{\mathrm{H}} + n_{\mathrm{L}})/2$ and the modal index difference $\Delta n = n_{\mathrm{H}} - n_{\mathrm{L}}$ are determined by ϵ_{x} and the waveguide widths, where n_{H} and n_{L} are the modal indices for the high- and low-index waveguide sections, respectively. Specifically, a larger ϵ_{x}, which can be achieved by a smaller d given a certain subwavelength a, will lead to a higher n_{eff} and thus a smaller grating period Λ.[3,20] Such a smaller Λ can avoid the radiation caused by the leaky-wave effect at higher frequencies, promising a broadband operation of the device. However, a higher ϵ_{x} could reduce the modal index difference Δn, leading to a smaller reflection depth and a narrower 3-dB bandwidth.[3,20] Therefore, the trade-offs for selecting the various parameters $(w_{\mathrm{H}}, w_{\mathrm{L}}, a, \text{and } d)$ must be considered in terms of operation bandwidth, device footprint, rejection level, and 3-dB bandwidth.

Considering the trade-offs mentioned above, with a priority to minimize the radiation at the upper bound of this WR-3.4 band, a larger relative permittivity for the cladding is preferred. To accommodate the grating profile well, a square lattice is adopted for the filter design as shown in Fig. 1(b). Thus, the perforation period together with the hole diameter for the square lattice has to be selected according to the grating period. To satisfy the subwavelength perforation period condition,[3,4,15,19] the initial perforation period a for the square lattice is selected as $\Lambda/4$ or equivalently $\lambda_{\mathrm{Bg}}/8$, where λ_{Bg} is the guided Bragg wavelength.[20] Given $l_{\mathrm{H}} = l_{\mathrm{L}} = \Lambda/2 = \lambda_{\mathrm{Bg}}/4$, where l_{H} and l_{L} are the lengths for the high- and low-index sections, respectively,[20] each waveguide section can hold two columns of holes along the z-direction. Given a certain ϵ_x and a, the hole diameter d can be calculated based on Eq. (1). Further reduction in a to obtain more holes per Bragg period would lead to very small holes, beyond the fabrication limit of around 20 μm, based on the standard deep reactive ion-etching (DRIE) process.[3] On the other hand, when increasing a to $\lambda_{\mathrm{Bg}}/4$, where only one column of holes would be accommodated by each waveguide section, a larger hole diameter d would be required to maintain the same air-in-silicon fill factor. However, the larger material discontinuities between air and silicon could cause wave scattering, while the device mechanical strength could be degraded.

To design a filter working at a Bragg frequency of 275 GHz with a 3-dB bandwidth around 16 GHz, we select the waveguide widths as $w_{\mathrm{H}} = 240$ μm and $w_{\mathrm{L}} = 100$ μm. Given $(\epsilon_x, \epsilon_y, \epsilon_z) = (6.64, 8.19, 6.64)$, the corresponding modal indices of n_{H} and n_{L} for the E_{11}^x mode are obtained as 2.66 and 2.32, respectively, based on port-mode simulations in CST. Correspondingly, the length for each waveguide section is calculated with approximations as $l_{\mathrm{H}} = l_{\mathrm{L}} = 111.5$ μm together with the perforation period $a = 55.8$ μm and hole diameter $d = 36$ μm. In this case, both waveguide sections have low insertion loss at lower frequencies,[3] while based on our initial investigations, such a waveguide difference allows for a strong rejection band with a relatively short total grating length, e.g., 1 cm. The detailed criteria on the selection of waveguide difference can be found in the supplementary material.

III. CHARACTERISTICS OF THE FILTER

In this section, various characteristics of the proposed filters are discussed, including transmission, 3-dB bandwidth, central frequency, and dispersion. A lateral multi-layer cladding is introduced for the first time to reduce the transmission fluctuation, while apodization is employed to mitigate the band transition ripples. The fabrication for various filters is based on the standard deep reactive-ion etching (DRIE) process, while several illustrative designs are experimentally validated.

A. Transmission performance

1. Uniform waveguide Bragg grating

Based on the descriptions in Sec. II, a uniform waveguide grating filter is realized as shown in Fig. 2. The filter consists of four major elements, including a tapered coupling structure, a regular waveguide, a transition waveguide, and a Bragg grating with a grating number $N_{\mathrm{g}} = 40$. The 3-mm coupling tapers are introduced for excitation purpose, i.e., they are inserted into the WR-3.4 rectangular hollow waveguides in both simulations and measurements so that the waves can be gradually coupled from the feed to the device. As shown in Figs. 2(b) and 2(c), a regular waveguide with a cladding effective relative permittivity of 2.75 is employed because it has a tight wave confinement and thus a better mode matching to the hollow waveguide than that of the waveguide cladded by the higher-index claddings. Thus, it can enhance the coupling between the filter and the feed. In addition, the regular waveguides allow consistent interconnection between the filter and other components on the same platform.

To provide good impedance matching between the regular waveguide section and the grating, a transition waveguide is adopted as illustrated in Figs. 2(d) and 2(e). Specifically, the hole diameter in the transition cladding decreases gradually, leading to an increasing modal index toward the grating. As shown in Fig. 2(f), the Bragg gratings are implemented with $w_{\mathrm{H}} = 240$ μm and $w_{\mathrm{L}} = 100$ μm, while the optimized grating period Λ is 223 μm. Correspondingly, the cladding configuration is $(a, d) = (55.8\ \mu\mathrm{m}, 36\ \mu\mathrm{m})$. Given $N_g = 40$, the total grating length is 8.92 mm. The claddings extend to 12 rows on both sides of the waveguide to accommodate the evanescent fields.

The fabricated sample is shown in Fig. 3. It is observed that the adjacent holes are slightly connected in the first two columns for the transition claddings due to the fabrication tolerance. Owing to the concept of effective medium, this imperfection has a negligible impact on the effective relative permittivity. The measurements are accomplished with the arrangement shown in Fig. 4 by using a

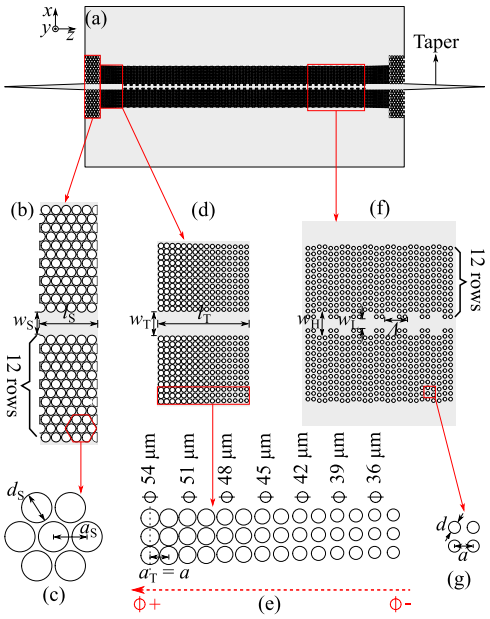

FIG. 2. Uniform effective-medium-clad waveguide Bragg grating filter. (a) Top view. (b) A regular effective-medium-clad waveguide with a core width w_S = 225 μm and length l_S = 500 μm. (c) The hexagonal lattice of the effective medium cladding for the regular waveguide with a lattice period a_S = 100 μm and hole diameter d_S = 90 μm. (d) The transition waveguide between the regular feeding waveguide and the Bragg grating with a core width w_T = 240 μm and length of l_T = 781 μm. (e) The effective medium cladding of the transition waveguide in a square lattice. (f) The uniform waveguide Bragg grating with a higher-index waveguide core width w_H = 240 μm, lower-index core width w_L = 100 μm, and grating period Λ = 223 μm. (g) The square lattice of the effective medium cladding for the Bragg grating with a lattice period a = 55.8 μm and hole diameter d = 36 μm. The tapered structures that are inserted into the WR-3.4 hollow waveguides in both simulations and measurements allow efficient coupling from the feed to the sample. The unpatterned silicon slab is for handling purpose. Slight systematic amendments of the dimensions are necessary to account for fabrication tolerances in the final results, as elaborated in the supplementary material.

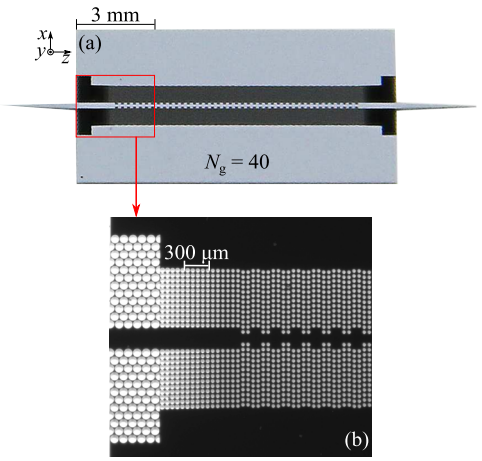

FIG. 3. Fabricated uniform effective-medium-clad Bragg grating filter. (a) The filter sample. (b) The microscope image revealing a regular waveguide, transition waveguide, and Bragg grating.

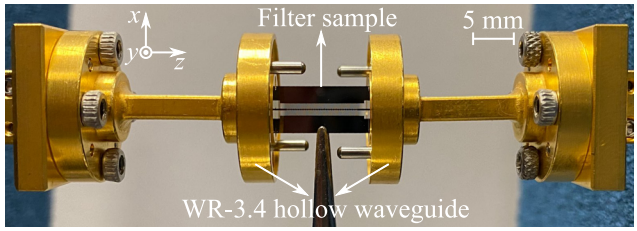

FIG. 4. Measurement setup. The tapered structures are inserted into the WR-3.4 hollow waveguides for excitation, while the sample is fixed by a holder at the unpatterned silicon slab. The WR-3.4 waveguide operates in the TE_{10} mode so that the E_{11}^x mode with polarization in the x-direction is excited for the filter sample. The measurements are conducted by using a Keysight vector network analyzer with VDI WR-3.4 extension modules spanning 220–330 GHz.

Keysight vector network analyzer with VDI WR-3.4 extension modules spanning from 220 to 330 GHz. The measured and simulated S-parameters are shown in Figs. 5(a) and 5(b) with good agreement. However, it is observed that the Bragg frequency is shifted to 280 GHz from the designed frequency of 275 GHz while the 3-dB bandwidth is slightly broadened by around 1 GHz. We found that such a 5-GHz blue shift and the increasing 3-dB bandwidth happen to all the samples in this work and they are mainly caused by an observed reduced wafer thickness from 250 μm and slightly over-etched holes. These causes are confirmed in the supplementary material, where the relevant dimensions are modified in simulation to compensate these systematic errors caused by the fabrication tolerances. It is noted that all the simulated results presented in the main text have been systematically corrected accordingly, and the compensated dimensions can be found in the supplementary material. From Fig. 5(a), a 3-dB bandwidth around 18 GHz is achieved with a stop-band rejection below −21 dB. There exists

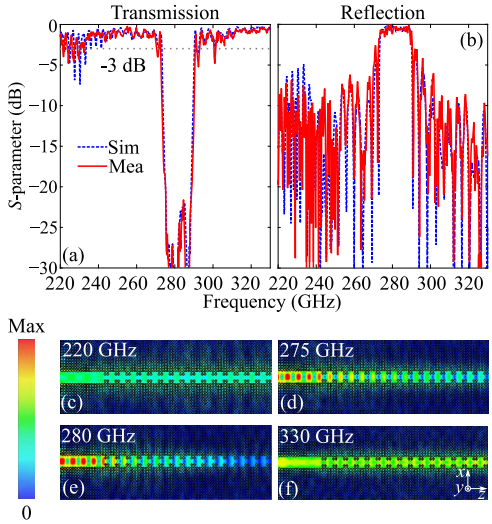

FIG. 5. Simulated and measured S-parameters and simulated E-field amplitude distributions of the uniform waveguide Bragg grating filter. (a) Transmission. (b) Reflection. E−field distributions at (c) 220, (d) 275, (e) 280, and (f) 330 GHz. All the E−field distributions are normalized by the same factor.

significant fluctuation in the pass bands especially at the lower frequencies and near the transition shoulders. The fluctuation at the low frequency is mainly due to the weak wave confinement, as shown in Fig. 5(c), resulting in a large field penetration depth into the claddings. Correspondingly, the field is disturbed by the nearby unetched silicon slab. On the other hand, the ripples at the transitions are mainly because of the strong reflection among the gratings. These issues are resolved Sec. III A 2 and III A 3.

2. Cladding effects

To investigate the effects of the claddings on the passband transmission, we design three gratings cladded by air,[21] by wider uniform effective medium claddings, and by two-layer mixed effective medium claddings, as shown in Figs. 6(a)–6(c). For the air-clad filter, to maintain a comparable 3-dB bandwidth and grating coupling strength, the waveguide widths are selected as w_{Ha} = 240 μm and w_{La} = 200 μm, resulting in a modal index difference of 0.47 at 275 GHz and a grating period Λ of 288 μm. With a longer Λ, we reduce the grating number N_g to 20 to achieve a comparable rejection depth and roll-off rate. This air-clad Bragg grating filter is fed by a straight regular waveguide as shown in Fig. 7(a). Figure 6(b) illustrates a uniform waveguide filter with a wider cladding containing 24 rows of holes, while the other parameters are the same as in Fig. 2. For further investigation, the wide uniform cladding is replaced with a two-layer mixed cladding as shown in Figs. 6(c)–6(e), where the outer layer with a lower index is formed in a hexagonal lattice with a_e = 100 and d_e = 90 μm, while the inner layer with a higher index

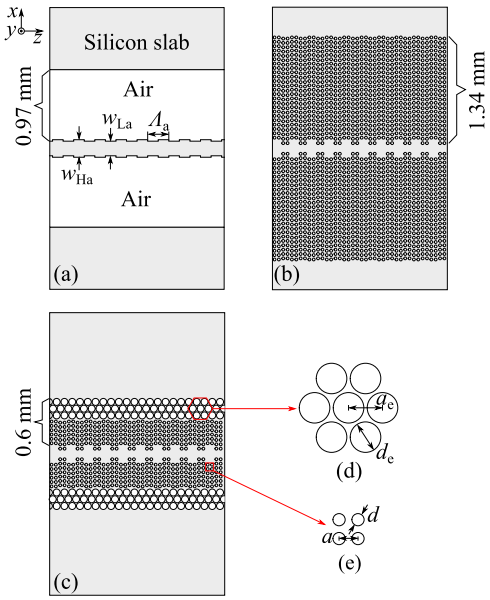

FIG. 6. Schematics of Bragg grating filters with various claddings. (a) The air-clad filter with a high-index waveguide width w_{Ha} = 240 μm, low-index waveguide width w_{La} = 200 μm, and grating period Λ_a = 288 μm. (b) The uniform effective-medium-clad filter with a cladding width of 1.34 mm containing 12 rows of holes. (c) A two-layer mixed cladding filter with a cladding width of 0.6 mm. (d) The hexagonal lattice of the outer cladding with a lattice period a_e = 100 μm and d_e = 90 μm. (e) The square lattice of the inner cladding with a lattice period a = 55.8 μm and d = 36 μm. The hole configuration of (b) is identical to that in Fig. 2(f).

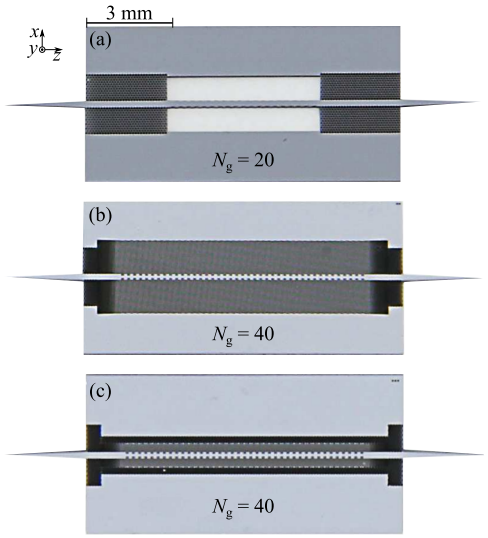

FIG. 7. Fabricated waveguide Bragg gratings with various claddings. (a) The air-clad filter sample. (b) The wide uniform effective-medium-clad filter sample. (c) The mixed effective-medium-clad filter sample. All subfigures share the same scale.

is built in a square lattice with a = 55.8 and d = 36 μm. The consideration to adopt two types of claddings in this work mainly includes structural completeness, mechanical strength, and fabrication tolerance. For the inner cladding, a square lattice is introduced to accommodate the square grating profile as discussed in the design consideration. For the outer cladding, a hexagonal lattice with a larger lattice period is adopted mainly because of the mechanical strength and fabrication tolerance. Specifically, the outer cladding has a much lower permittivity requiring larger air holes given a constant lattice period, which could lead to weakened mechanical strength. In this case, a hexagonal lattice is preferred to enhance the mechanical strength. In addition, with an identical fill factor of air volume in silicon, a larger lattice period can result in a larger spacing between the edges of the adjacent holes so as to avoid hole merging due to the over-etching in fabrication. The fabricated samples of the three filters are shown in Fig. 7.

The simulated and measured S-parameters of the air-clad filter are shown in Figs. 8(a) and 8(b). Obviously, the passband fluctuation is reduced significantly due to a stronger wave confinement resulting from a larger refractive index contrast between the air cladding and the silicon waveguide. Thus, there is negligible interference with the nearby unetched silicon slab. In addition, the transition level is improved to above −3 dB due to the smaller grating number, resulting in weaker reflection. However, the transmission level at lower frequencies is decreased to below −3 dB, which is caused by the impedance mismatch between the feeding and the grating waveguide with a modal index difference of around 0.5 from 220 to 235 GHz. Meanwhile, a relatively stronger loss is also observed at higher frequencies. This is because the grating period is larger than the guided wavelength, leading to radiation akin to a leaky wave antenna.[22] In general, these effects are common for the conventional Bragg grating filters cladded by air or silicon dioxide, and they result in a reduced operation bandwidth. In the next case,

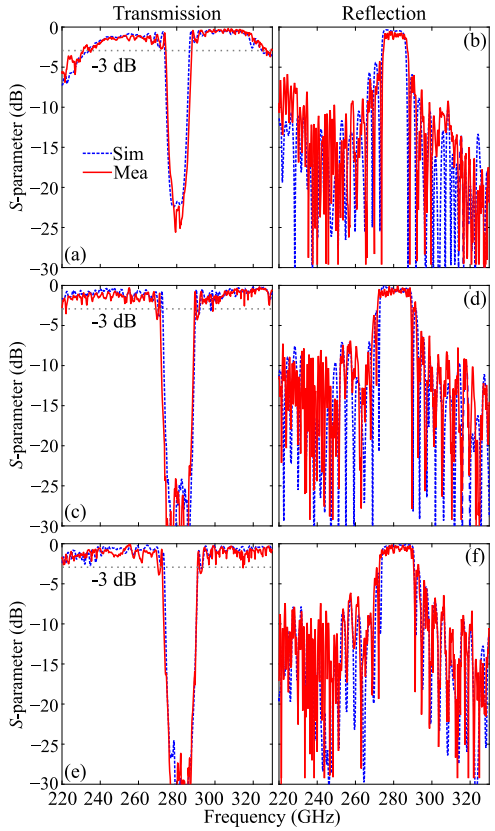

FIG. 8. Simulated and measured *S*-parameters of the filters with different claddings. (a) and (b) The air-clad filter. (c) and (d) The wide uniform cladding filter. (e) and (f) The two-layer mixed cladding filter.

as indicated in Figs. 8(c) and 8(d), we see that a wider effective medium cladding that is able to accommodate extended evanescent fields can also alleviate the passband fluctuation. However, expanding the cladding reduces the structural compactness considerably. In contrast, as illustrated in Figs. 8(e) and 8(f), the two-layer mixed claddings can achieve a comparable transmission level but with only half the cladding width. Here, the outer layer confines the evanescent fields mainly within the two-layer claddings due to their relatively large refractive index contrast. In this case, the disturbance from the silicon slab is reduced, resulting in a smoother transmission level. However, the transition shoulders are still lower than −3 dB with such a configuration, and this issue is addressed in Sec. III A 3.

3. Apodized waveguide Bragg grating

To reduce the fluctuation around the transitions, an apodization technique is employed to gradually increase the grating coupling coefficient.[23–25] Based on the coupled-mode theory, the coupling coefficient κ representing the amount of reflection per unit length is defined as[20]

$$\kappa = \frac{2\Delta n}{\lambda_{B0}}, \tag{4}$$

where Δn is the grating modal index difference and λ_{B0} is the Bragg wavelength in free space. This apodization technique has been widely used in designing optical fiber and waveguide grating structures,[23–25] and there are a number of window functions with various roll-off rates available to taper the coupling strength such as linear ramp, raised-cosine, Hamming, or Gaussian functions. However, the trade-offs in terms of the transition level, filter roll-off rate, and device footprint have to be considered. A window function with a smaller roll-off rate can generate a smoother transition. However, it requires a large number of periods and thus a longer footprint to achieve a comparable stop-band level as its counterpart without apodization.

Considering the trade-offs discussed above, in this work, we use a linear ramp function to taper the coupling strength. The realized filter with apodization is shown in Figs. 9(a)–9(c). The key parameters are kept the same as in the two-layer-cladding design in Fig. 6(c), while the grating in the first ten periods is apodized symmetrically. As depicted in Fig. 9(c), the waveguide width difference is gradually increased from $0.1\Delta w$ to Δw in a step of $0.1\Delta w$, where $\Delta w = w_H - w_L$. Therefore, the modal index difference Δn is gradually increased correspondingly. Thus, the coupling coefficient κ is tapered physically so as to achieve a moderately strong reflection at the transition band. The fabricated sample and

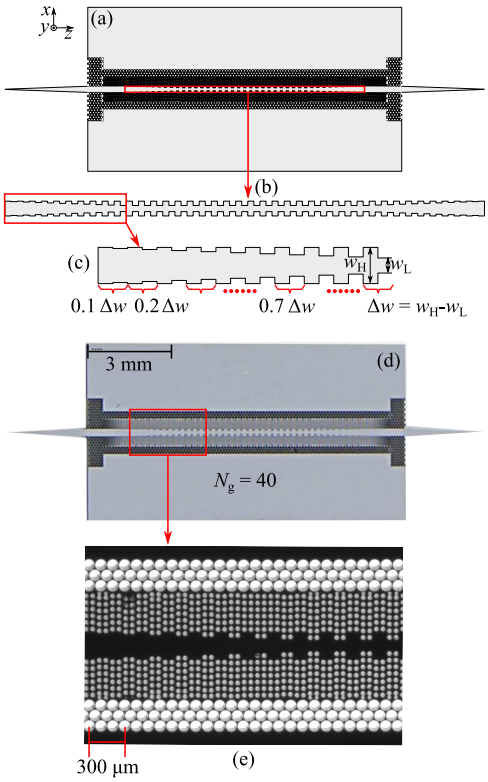

FIG. 9. Bragg grating filter with apodization. (a) The apodized filter cladded by the two-layer mixed effective medium cladding. (b) The Bragg grating. (c) The apodized part. (d) The fabricated filter with apodization. (e) The microscope image around the grating with apodization.

a magnified view containing various critical features are shown in Figs. 9(d) and 9(e).

As shown in Figs. 10(a) and 10(b), when applying the apodization, the filter can achieve fluctuation near transitions of around −2 dB, while the stopband level is reduced compared to the one without apodization shown in Fig. 8(e). These results match the expectations. In addition, assisted by the mixed claddings, the filter achieves smooth passband transmission levels together with a 3-dB bandwidth of 18.5 GHz. The roll-off rate calculated between −3 and −20 dB is 4.42 dB/GHz, resulting in good frequency selectivity. Indeed, the transition level can be further enhanced by using a deeper apodization function, e.g., cosine function, but at the expense of a stopband level or structural compactness.

B. Bandwidth

To vary the 3-dB bandwidth, the grating modulation can be modified.[20] According to the bandwidth equation,[20]

$$\Delta\lambda = \frac{\lambda_{B0}^2 \kappa}{\pi n_g}, \tag{5}$$

where n_g is the group index, and the filter bandwidth is mainly determined by the coupling coefficient κ that is proportional to the modal index difference Δn, as expressed in Eq. (4). Accordingly, given a fixed w_H, a narrower and a broader bandwidth are obtained by increasing or decreasing w_L, respectively. As shown in Figs. 11(a) and 11(b), the filter with a broader bandwidth has a stronger stopband, while the transition level is steeper. These phenomena originate from a smaller average modal index n_{eff} that can lead to a larger grating period and thus a longer total length L, given a constant grating number.[20]

Alternatively, the 3-dB bandwidth also can be adjusted by varying the cladding relative permittivity, while maintaining the grating configuration. For the second strategy, we select w_H = 240 μm and w_L = 100 μm for both filters, while the effective relative permittivity of the inner cladding ϵ_{inner} is either 7.93 or 5.32. Here, the relative permittivity of the outer cladding is maintained at 2.75. The measured and simulated S-parameters as shown in Figs. 11(c) and 11(d) illustrate that the filter with a lower-index inner cladding achieves a broader bandwidth and stronger rejection depth. This is because a lower-index cladding can reduce the average waveguide modal

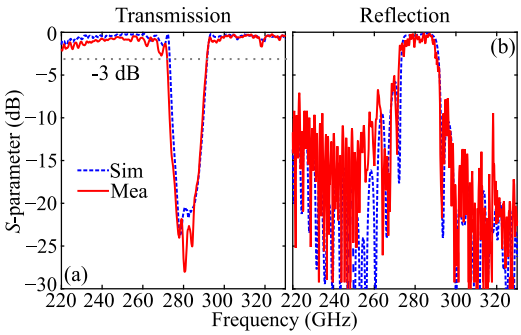

FIG. 10. Simulated and measured S-parameters of the filter with apodization and the two-layer mixed cladding. (a) Transmission and (b) reflection.

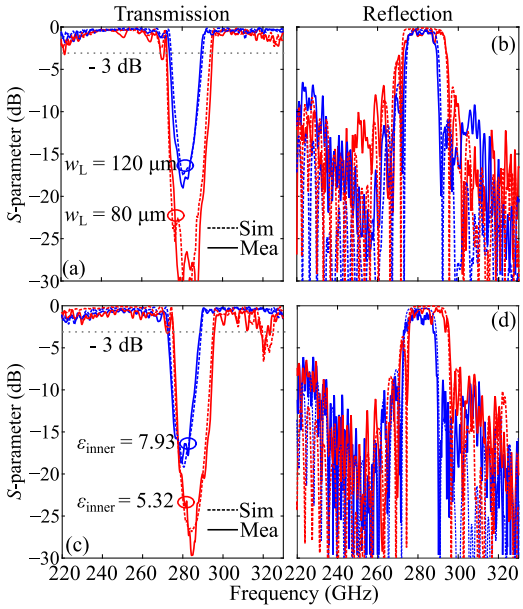

FIG. 11. Simulated and measured S-parameters of the filter clad by mixed effective medium claddings with various bandwidths achieved by different strategies. (a) Transmission and (b) reflection for the filters with different widths of the lower-index waveguide section, while the higher-index waveguide width is maintained at 240 μm. (c) Transmission and (d) reflection for the filters, where the inner cladding relative permittivity is varied, while the outer cladding has a constant relative permittivity of 2.75. For fair comparisons, all the gratings are linearly apodized and cladded by two-layer mixed effective medium claddings with a grating number N_g = 40.

index n_{eff}, while enhancing the modal index contrast Δn, leading to a larger κ and thus a broader bandwidth from Eqs. (4) and (5). However, a sudden drop in S_{21} appears at around 320 GHz, which is mainly due to the mode radiation caused by the longer grating period. This could be remedied by optimizing the waveguide widths together with the cladding configuration.

C. Central frequency

To demonstrate that the proposed filter type is tailorable to operate across the whole WR-3.4 band, filter performances with Bragg frequencies shifted to 310 and 250 GHz are presented. These filters are in the form of apodized grating cladded by the two-layer mixed claddings with a relative permittivity of 2.75 and 6.64 for the outer and inner claddings, respectively. To achieve comparable 3-dB bandwidth and rejection, the higher-index waveguide width w_H is maintained constant at 240 μm, while the lower-index waveguide width w_L is set at 110 μm and 90 μm for the higher and lower Bragg frequencies, respectively. Accordingly, the grating periods are calculated as 192 μm and 264 μm for the higher and lower frequencies, respectively, while the grating number is kept at 40 for both designs. The simulated and measured S-parameters are shown in Figs. 12(a)–12(d). Attributed to its relatively small grating coupling strength, the filter operating at the higher frequency can achieve a smooth passband transmission level and a rejection depth below −17 dB. However, for the lower-frequency one, the transition level at

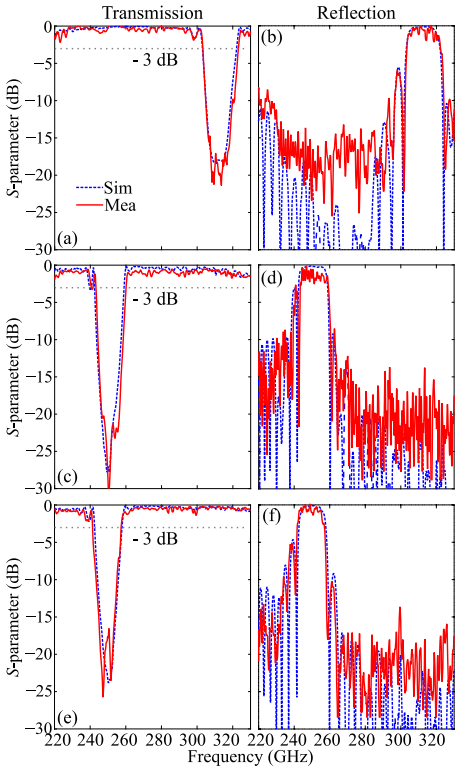

FIG. 12. Simulated and measured *S*-parameters of the filters cladded by mixed claddings with various Bragg frequencies. (a) Transmission and (b) reflection of the filter working at 310 GHz. (c) Transmission and (d) reflection of the filter working at 250 GHz with an inner cladding relative permittivity of 6.64. (e) Transmission and (f) reflection of the filter working at 250 GHz with an inner cladding relative permittivity of 7.93.

the left shoulder is reduced to below −3 dB due to the stronger coupling strength. It is noteworthy that the transmission level decreases with increasing frequency. This is mainly caused by the radiation loss due to the wavelengths becoming shorter than the grating period, thus leading to a leaky mode. This issue is typically not encountered in optical filters due to a much narrower bandwidth.

To minimize the radiation, a smaller grating period is required together with wavelength shortening so to maintain the center frequency. Accordingly, we implement a higher-index inner cladding with a relative permittivity of 7.93 and a reduced w_L of 80 μm to maintain a comparable 3-dB bandwidth. As a result, the grating period is reduced to 250 μm, as opposed to 264 μm. According to Figs. 12(e) and 12(f), the transmission levels at higher frequencies are improved with a transition level well above −13 dB. These results further show that the proposed filter type can operate in a 40% fractional bandwidth that is much larger than any practical optical band.

D. Dispersion

To investigate the dispersion characteristics of the proposed Bragg grating filters, we have simulated and measured the group delay for a uniform filter and an apodized filter with mixed

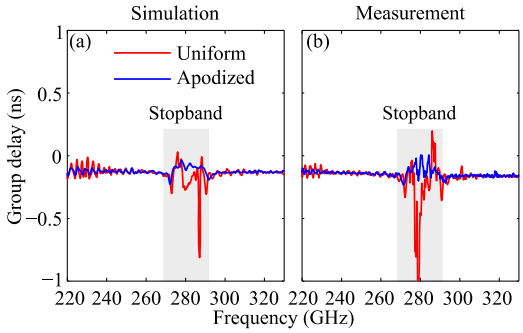

FIG. 13. Simulated and measured group delay of the uniform filter shown in Fig. 2 and the apodized filter with mixed claddings shown in Fig. 9. (a) Simulation. (b) Measurement. The group delays in both simulations and measurements are derived from the unwrapped phase, where the phase contributions introduced by the hollow waveguides and straight waveguide sections have been de-embedded by comparing the phase differences of the straight effective-medium-clad waveguides with multiple lengths. To mitigate the amplifying effects of the derivative operation on the phase noise, a smoothing function has been employed to process the measured data with a sliding window covering 1 GHz.

claddings. As shown in Fig. 13, the measurements agree well with the simulations, where both filters show a small fluctuation in the group delay across the passband. The measured group delay for the apodized filter varies from −0.12 to −0.17 ns across the entire passband, demonstrating an extremely low dispersion. For the uniform filter, the group delay is relatively higher with fluctuations at the lower passband. This is mainly caused by the external disturbance, i.e., the interference with the nearby unetched silicon slab. The results further show that the mixed claddings together with the apodization can reduce the filter dispersion. In general, the proposed Bragg grating filters inherit the low dispersion of the effective-medium-clad waveguides, allowing for broadband operation. This is crucial to terahertz communications with high-speed data transmission.

IV. CONCLUSION

A class of integrated waveguide Bragg grating filters based on all-silicon effective-medium-clad waveguides has been comprehensively investigated. Various filter characteristics, including transmission level, 3-dB bandwidth, and Bragg frequency, have been considered over a wide operation frequency range from 220 to 330 GHz (WR-3.4 band). The filters are made in a substrateless high-resistivity float-zone silicon wafer based on the standard deep reactive-ion etching process. Relying on their tailorable effective medium claddings that are realized by periodically perforating the silicon slab, the proposed Bragg grating filter type has an additional degree of flexibility to control the performance compared with the conventional silicon-on-insulator (SOI) ones. By applying the apodization technique, the transition level is improved to above −3 dB. Importantly, two-layer mixed effective medium claddings with different relative permittivities are introduced to improve the passband transmission levels to above −1.5 dB with average ripples less than 0.5 dB, while maintaining the lateral footprint within one wavelength. Furthermore, the combination of hybrid claddings

and apodization can further reduce the dispersion, with a measured group delay varying between −0.12 and −0.17 ns across the whole passband. The radiation loss at higher frequencies for a grating with a long period is minimized by introducing higher-index effective medium claddings, thus allowing for a broadband operation. With high efficiency, low dispersion, and broad bandwidth, the proposed filter type is applicable at high terahertz frequencies, e.g., above 1 THz, as detailed in the supplementary material. It can be foreseen that such Bragg grating structures can be implemented together with other components on this substrateless integrated platform for a wide range of terahertz applications. The presented effective medium techniques can also be adopted in optics for enhancing filter performance.

SUPPLEMENTARY MATERIAL

The supplementary material includes the impact of waveguide difference Δw, fabrication tolerance, frequency shift caused by fabrication tolerance, and applicability at high terahertz frequencies.

ACKNOWLEDGMENTS

This work was supported by the Australian Research Council Discovery Project under Grant No. ARC DP180103561. The authors would like to thank C. Wang for photographing the samples. The samples were fabricated by Silicon Sensing Systems Japan Ltd. The Quadro P6000 GPU used for this research was contributed by NVIDIA Corporation.

DATA AVAILABILITY

The data that support the findings of this study are available within the article and its supplementary material.

REFERENCES

[1]K. Sengupta, T. Nagatsuma, and D. M. Mittleman, "Terahertz integrated electronic and hybrid electronic–photonic systems," Nat. Electron. **1**(12), 622–635 (2018).
[2]W. Withayachumnankul, M. Fujita, and T. Nagatsuma, "Integrated silicon photonic crystals toward terahertz communications," Adv. Opt. Mater. **6**(16), 1800401 (2018).
[3]W. Gao, W. S. Lee, X. Yu, M. Fujita, T. Nagatsuma, C. Fumeaux, and W. Withayachumnankul, "Characteristics of effective-medium-clad dielectric waveguides," IEEE Trans. Terahertz Sci. Technol. **11**(1), 28–41 (2020).
[4]W. Gao, X. Yu, M. Fujita, T. Nagatsuma, C. Fumeaux, and W. Withayachumnankul, "Effective-medium-cladded dielectric waveguides for terahertz waves," Opt. Express **27**(26), 38721–38734 (2019).
[5]W. Gao, C. Fumeaux, and W. Withayachumnankul, "All-silicon terahertz components towards efficient integrated systems," in *2020 45th International Conference on Infrared, Millimeter, and Terahertz Waves (IRMMW-THz)* (IEEE, 2020), pp. 1–2.
[6]D. M. Pozar, *Microwave Engineering* (John Wiley & Sons, 2011).
[7]H. A. Macleod, *Thin-Film Optical Filters* (CRC Press, 2017).
[8]F. Wang, V. F. Pavlidis, and N. Yu, "Miniaturized SIW bandpass filter based on TSV technology for THz applications," IEEE Trans. Terahertz Sci. Technol. **10**(4), 423–426 (2020).
[9]Z. Chen, Y. Zheng, X. Kang, B. Lu, and B. Cui, "WR-2.8 band micromachined rectangular waveguide filter," J. Infrared, Millimeter, Terahertz Waves **34**(12), 847–855 (2013).
[10]Z. Xing-Hai, Z. Ying-bin, S. Guang-cun, C. Yong-sheng, B. Jing-fu, S. Chan-hung, Z. Hao-shen, and D. Yi-jia, "G-band rectangular waveguide filter fabricated using deep reactive ion etching and bonding processes," Micro Nano Lett. **7**(12), 1237–1240 (2012).
[11]W. Withayachumnankul, B. M. Fischer, and D. Abbott, "Quarter-wavelength multilayer interference filter for terahertz waves," Opt. Commun. **281**(9), 2374–2379 (2008).
[12]H. Li, S. Atakaramians, J. Yuan, H. Xiao, W. Wang, Y. Li, B. Wu, and Z. Han, "Terahertz polarization-maintaining subwavelength filters," Opt. Express **26**(20), 25617–25629 (2018).
[13]E. Akiki, M. Verstuyft, B. Kuyken, B. Walter, M. Faucher, J.-F. Lampin, G. Ducournau, and M. Vanwolleghem, "High Q THz photonic crystal cavity on a low loss suspended silicon platform," IEEE Trans. Terahertz Sci. Technol. **11**(1), 42–53 (2020).
[14]D. T. H. Tan, K. Ikeda, and Y. Fainman, "Cladding-modulated Bragg gratings in silicon waveguides," Opt. Lett. **34**(9), 1357–1359 (2009).
[15]P. Cheben, R. Halir, J. H. Schmid, H. A. Atwater, and D. R. Smith, "Subwavelength integrated photonics," Nature **560**(7720), 565–572 (2018).
[16]X. Wang, W. Shi, R. Vafaei, N. A. Jaeger, and L. Chrostowski, "Uniform and sampled Bragg gratings in SOI strip waveguides with sidewall corrugations," IEEE Photonics Technol. Lett. **23**(5), 290–292 (2010).
[17]X. Wang, W. Shi, H. Yun, S. Grist, N. A. Jaeger, and L. Chrostowski, "Narrow-band waveguide Bragg gratings on SOI wafers with CMOS-compatible fabrication process," Opt. Express **20**(14), 15547–15558 (2012).
[18]X. Wang, S. Grist, J. Flueckiger, N. A. F. Jaeger, and L. Chrostowski, "Silicon photonic slot waveguide Bragg gratings and resonators," Opt. Express **21**(16), 19029–19039 (2013).
[19]A. V. Subashiev and S. Luryi, "Modal control in semiconductor optical waveguides with uniaxially patterned layers," J. Lightwave Technol. **24**(3), 1513–1522 (2006).
[20]L. Chrostowski and M. Hochberg, "Waveguide Bragg grating filters," in *Silicon Photonics Design: From Devices to Systems* (Cambridge University Press, 2015), pp. 117–143.
[21]D. Headland, W. Withayachumnankul, X. Yu, M. Fujita, and T. Nagatsuma, "Unclad microphotonics for terahertz waveguides and systems," J. Lightwave Technol. **38**(24), 6853–6862 (2020).
[22]D. Headland, Y. Monnai, D. Abbott, C. Fumeaux, and W. Withayachumnankul, "Tutorial: Terahertz beamforming, from concepts to realizations," APL Photonics **3**(5), 051101 (2018).
[23]T. E. Murphy, *Design, Fabrication and Measurement of Integrated Bragg Grating Optical Filters* (Massachusetts Institute of Technology, 2001).
[24]X. Wang, *Silicon Photonic Waveguide Bragg Gratings* (University of British Columbia, 2013).
[25]A. Othonos, K. Kalli, D. Pureur, and A. Mugnier, "Fibre Bragg gratings," in *Wavelength Filters in Fibre Optics* (Springer, 2006), pp. 189–269.